12-2019

Helium in Stream Water as a Volcanic Monitoring Tool

W. Payton Gardner

David D. Susong

Geochemistry, Geophysics, Geosystems

AGU100 ADVANCING EARTH AND SPACE SCIENCE

RESEARCH ARTICLE
10.1029/2019GC008698

Special Section:
FRONTIERS IN GEOSYSTEMS: Deep Earth - surface interactions

Helium in Stream Water as a Volcanic Monitoring Tool

W. Payton Gardner[1] **and David D. Susong**[2]

[1]Department of Geosciences, University of Montana, Missoula, MT, USA, [2]Utah Water Science Center, USGS Emeritus, West Valley City, UT, USA

Key Points:
- Volcanic helium can be measured in stream water
- Stream water can be used to estimate groundwater helium isotopic composition
- Stream water can be used to monitor volcanic volatiles in groundwater

Correspondence to:
W. Payton Gardner,
payton.gardner@umontana.edu

Citation:
Gardner, W. P., & Susong, D. D. (2019). Helium in stream water as a volcanic monitoring tool.. *Geochemistry, Geophysics, Geosystems*, *20*, 6000–6015. https://doi.org/10.1029/2019GC008698

Received 16 SEP 2019
Accepted 24 NOV 2019
Accepted article online 26 NOV 2019
Published online 10 DEC 2019

Abstract We show that synoptic sampling of streams can be used to characterize volcanic volatiles in groundwater over large spatial scales. Synoptic sampling of dissolved noble gases, ^{222}Rn, major ions, and stream discharge was carried out along a 30 km reach of the Gibbon River, near Norris Geyser Basin in Yellowstone National Park, USA. Groundwater discharge location, volume, and composition were estimated by constrained calibration of a stream flow and solute transport model. Estimated groundwater composition from stream modeling was compared to shallow groundwater concentrations measured in nearby springs. ^{3}He, ^{222}Rn, and Cl^{-}_{aq} signatures in the Gibbon River are indicative of groundwater discharge with a volcanic signature along the study reach. Stream water noble gas isotopic composition has similar isotopic mixing patterns to springs. The model-estimated composition of groundwater discharging to the Gibbon agrees well with observed groundwater composition from nearby springs for all modeled analytes. We present the first observations of elevated mantle helium in stream water and show that stream water can be used as a convenient collection point to estimate spatially distributed groundwater composition and to monitor changes in volatile flux over large spatial areas. These results offer the possibility that stream surveys in volcanic terrain could be a new method for distributed volcanic monitoring at the catchment scale and beyond.

1. Introduction

The spatial distribution of volcanic volatiles in groundwater has been shown to provide information on a variety of volcanic processes including: passive degassing (Ohwada et al., 2012), volcanic fluid movement (Aizawa et al., 2016), and local to regional strain and seismicity (Sano et al., 2015; Padrón et al., 2013; Kennedy and van Soest, 2007). In particular, helium isotopic ratios of groundwater have been shown to respond to both volcanic disturbance (Padrón et al., 2013) and seismic deformation (Brauer et al., 2003). However, groundwater sampling locations are normally limited to boreholes and springs. Boreholes provide point access to samples of the groundwater composition; however, dangerous drilling conditions, remote locations, and rugged topography often limit the number and location of such access points. Springs are an integrated sample of the groundwater system that feeds them Manga (2001), but are limited to special hydrogeological settings. Methods of monitoring the distributed groundwater helium isotope composition would greatly improve the spatial coverage of monitoring, and more convenient sampling locations could lead to improved temporal resolution.

Volcanic systems are characterized by highly fractured pyroclastic and magmatic deposits. These volcanic rocks often have high permeability and host shallow groundwater systems with large storage and circulation volumes (Gardner et al., 2010a; Manga, 1996; Ingebritsen and Scholl, 1993). Volcanic fluids and heat ascending to the surface are subject to transport by local groundwater systems, which exert first-order control on the location and magnitude of heat and volatile flux at the surface (Allard et al., 1997; Gardner et al., 2013; Hutnak et al., 2009; Hurwitz et al., 2003, 2002).

Helium isotopic ratios in groundwater are a powerful tool for monitoring volcanic processes (e.g., Crankshaw et al. 2018; Lowenstern et al. 2014; Morikawa et al., 2008; Sano et al. 2015). Helium is added to groundwater from volcanic, crustal, and atmospheric reservoirs in volcanic systems (Saar et al., 2005), with each reservoir having its own distinct isotopic signature (Ballentine et al., 2002). Groundwater flow can distribute volcanic volatiles, including helium, tens to hundreds of kilometers away from a volcanic center (Saar et al., 2005). Helium isotopes in groundwater systems can be used to monitor passive degassing in volcanic systems with little fumarolic activity (Ohwada et al., 2012). Recent studies have shown magmatically

derived helium in groundwater responds in precursory manner to volcanic activity (Padrón et al., 2013; Sano et al., 2015) and could potentially be a monitoring signal of volcanic unrest if the frequency and latency of groundwater analyses can be improved.

Groundwater helium is a potential indicator of stress, strain, and seismicity in volcanic systems where subsurface fluid pressure and stress are tightly coupled. Dilation, microfracture, and macroscopic failure break crystal lattices and create new transport pathways to release accumulated radiogenic ^{4}He into adjacent pore networks and groundwater (Bauer et al., 2019; Bauer, Gardner, & Lee, 2016; Bauer, Gardner, & Heath, 2016). The release of helium due to mechanical deformation during seismic events has been shown to alter helium isotopic composition of groundwater (Brauer et al., 2003). Regionally, helium in groundwater is influenced by tectonics and deformation. Large-scale ductile thinning of the crust allows for the leakage of mantle helium into crustal reservoirs in extensional terrains (Kennedy and van Soest, 2007), and brittle deformation in calderas can release virtually all accumulated crustal helium on geologic timescales (Lowenstern et al., 2014). The volume and dynamics of the helium release signal can be used as a quantitative indicator of mechanical deformation and the resulting changes in subsurface flow and transport properties (Gardner et al., 2017).

While groundwater isotopic and chemical composition contains useful information in volcanic settings, limited access limits the spatial and temporal coverage of sampling. Stream systems in volcanic terrains are highly connected to adjacent groundwater systems and often dominated by groundwater discharge (Gardner et al., 2010a; Manga, 1996). Streams integrate groundwater from a broad distribution of flow paths and flow scales. This integrated measurement has been exploited as a tool to monitor caldera wide hydrothermal flux (Friedman and Norton, 1990; McCleskey et al., 2016; Norton and Friedman, 1985). By synoptically sampling the stream network at higher spatial and temporal resolution, hydrothermal flux and geochemical processes can be resolved for specific watersheds and hydrothermal basins (Hurwitz et al., 2007; McCleskey et al., 2016). River solutes have been shown change temporally due to local hydrologic conditions (Friedman and Norton, 1990; Hurwitz et al., 2007) and well correlated to long-term heat flux (Ingebritsen et al., 2001).

Helium is a relatively new tracer in groundwater-stream water investigations. Groundwater discharge can change the helium content and isotopic composition of a river near the discharge point. Excess crustal ^{4}He has been observed in several stream systems as the result of deep regional groundwater discharge (Gardner et al., 2011a; Smerdon et al., 2012). By combining synoptic surveys of stream discharge, stream noble gas, and major ion chemistry, Beisner et al. (2018) show that the helium composition of deep, regional groundwater can be estimated from in-stream measurements. In volcanic systems such as Yellowstone, where groundwater contains excess magmatically derived ^{3}He and released crustal ^{4}He (Lowenstern et al., 2014), synoptic stream surveys could potentially be used as a method for sampling the distributed groundwater helium composition; however, excess ^{3}He in stream water has not been reported to date.

In this study, we combine synoptic measurements of stream discharge, Cl^-_{aq}, ^{222}Rn, and dissolved noble gas isotopes to estimate the spatial distribution, volume, and helium isotopic signature of groundwater discharging to the Gibbon River in Yellowstone National Park. We assess the use of synoptic stream surveys to provide information on the groundwater helium composition by comparing estimated groundwater composition to ~30 groundwater springs in the greater Norris area. The use of synoptic stream surveys provides an efficient method to rapidly sample groundwater helium composition over a broad spatial extent, while the integrated measurement provided by rivers is ideal for long-term monitoring of total volatile flux. Thus, this combined approach has the potential to provide significant new data for monitoring changes in passive degassing, volcanic volatile fluxes, and the state of stress and strain in volcanic systems around the world.

2. Study Area

The Gibbon River drains a 326 km^2 area along the northern boundary of the 640 ka Lava Creek caldera in Yellowstone National Park (Figure 1). The watershed has an average elevation ~2,000 m, with a mean annual temperature of 4 °C (Despain, 1987). About 70% of annual precipitation comes as winter snowfall, and the stream discharge pattern is dominated by spring snow melt (Gardner et al., 2010a). Streams on the Yellowstone volcanic plateau have high baseflow indices and anomalously low peak-flow to base-baseflow ratios, indicative of large volumes of groundwater discharge (Gardner et al., 2010a). Groundwater discharge

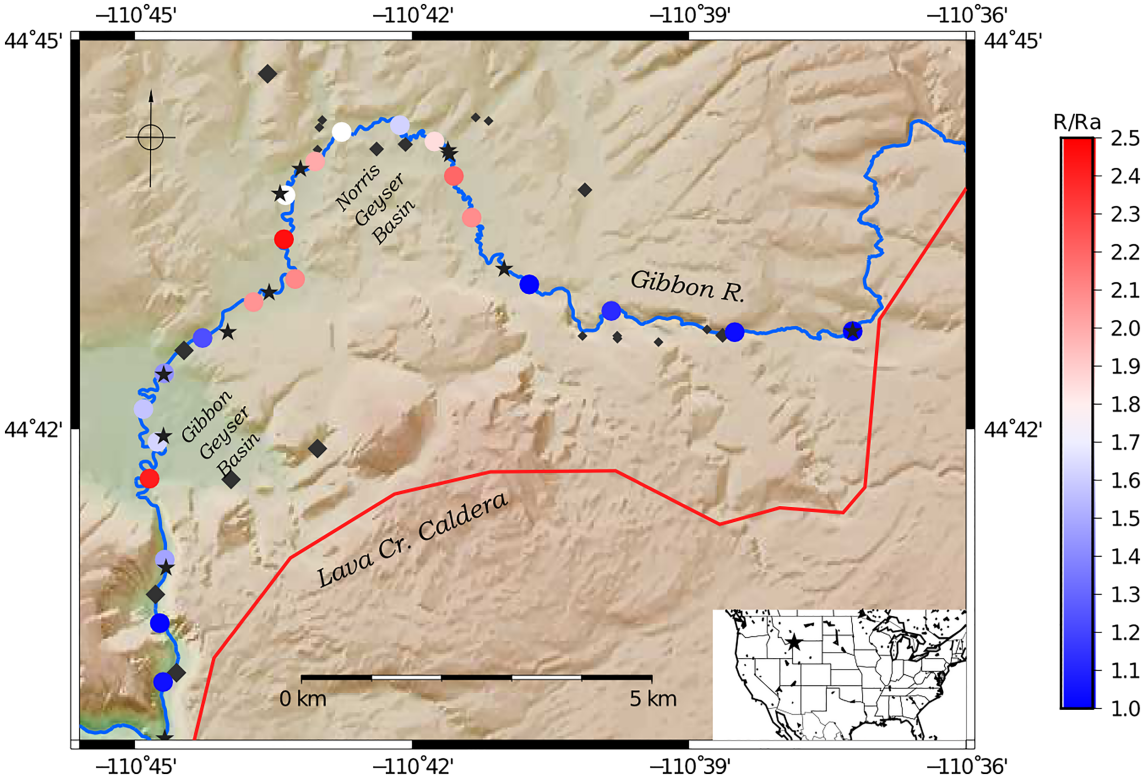

Figure 1. Map of the Gibbon River Study area. River samples plotted as circles colored by the sample helium R/R_a ratio. Spring samples plotted as diamonds scaled by helium R/R_a ratio. Small symbols have helium R/R_a ratio < 4, medium symbols have $4 \geq R/R_a \leq 7$, and large symbols have $R/R_a \geq 7$. Discharge measurements are marked by stars. The 600 ka Lava Creek Caldera boundary is shown in red.

in the basin comes from a variety of sources including deep, regional hydrothermal circulation, which mixes to various extents with shallow, cool, local groundwater systems (Gardner et al., 2013, 2011a, 2010b). The main hydrothermal reservoir is hosted between 3 and 5 km at temperatures around 350 °C (Gardner et al., 2013; Fournier, 1989). This hydrothermal water ascends and mixes with shallow groundwater flow occurring in fractured, silicic pyroclastic tuffs and rhyolitic lava flows (Gardner et al., 2013, 2011a, 2010a).

The Gibbon River flows around the Norris and Gibbon Geyser Basins over the studied reach (Figure 1). The Norris Geyser Basin is one of the major hydrothermal basins in Yellowstone National Park and is home to the highest measured surface and subsurface temperatures in the Park (Allen and Day, 1935; White et al., 1975). The acid-chloride springs in Norris have some of the most unique chemistry in the world (White et al., 1988). Hydrothermal discharge in Norris is a mixture of neutral-chloride water ascending from the deep hydrothermal reservoir and local shallow water heated by steam and volcanic volatiles produced by boiling during hydrothermal ascent (Fournier, 1989). Tantalus Creek drains the main hydrothermal basin and represents the majority of the hydrothermal discharge (White et al., 1988). The Gibbon Geyser Basin, downstream along the Gibbon from Norris (Figure 1), has significantly lower hydrothermal discharge and is dominated by steam discharge and acid-sulfate springs.

3. Theory

Groundwater discharge to rivers alters stream chemistry due to the difference in chemical and isotopic composition of groundwater and surface water. Surface water originating as precipitation is dilute and has a dissolved gas composition in equilibrium with the atmosphere. In the subsurface, groundwater dissolves minerals due to water-rock interaction and is exposed to naturally occurring radioactive decay chains, changing the chemical and isotopic composition. In Yellowstone, chemical weathering of minerals, mechanical damage of rocks and minerals, and addition of magmatic volatiles cause increasing concentrations in groundwater of several dissolved constituents used in this study including: chloride, helium, and radon.

3.1. Noble Gas Geochemistry

The equilibrium concentration of noble gases in water in contact with the atmosphere is set by the temperature, pressure (elevation), and addition of excess air at recharge (Aeschbach-Hertig et al., 2000, 2008). As groundwater moves away from the water table, it is isolated from the atmosphere and exposed to radiogenic materials in the Earth's crust and can mix with magmatic fluids. Several noble gas isotopes, for example, ^{36}Ar and ^{20}Ne, do not have significant subsurface sources, thus have concentrations that do not change if there is not significant interaction with a secondary phase.

Naturally occurring U and Th in crustal rocks produce radiogenic noble gas isotopes such as ^{222}Rn and ^{4}He. ^{222}Rn concentrations in water at equilibrium with the atmosphere are zero but are elevated in groundwater, providing an indicator of groundwater discharge to streams (Cook et al., 2003, 2006; Wanninkhof et al., 1990). The concentration of ^{222}Rn in groundwater reaches secular equilibrium for transport times longer than ~2 weeks. The equilibrium concentration depends upon the local production rate and transfer mechanics from the mineral to adjacent pore water (Torgersen, 1980).

Radiogenic ^{4}He is added to groundwater in volcanic systems due to alpha decay in crustal minerals and subsequent release to adjacent groundwater due to chemical weathering, mechanical deformation, and mineral diffusion (Torgersen, 1980). In volcanic systems, magmatic ^{3}He can be added both from active and passive gas release (Lowenstern et al., 2014; Ohwada et al., 2012; Padrón et al., 2013; Sano et al., 2015). The helium budget for a given isotope can be written

$$[^{i}He] = [^{i}He]_{\mathrm{atm}} + [^{i}He]_{\mathrm{rad}} + [^{i}He]_{\mathrm{m}}, \tag{1}$$

where $[^{i}He]_{\mathrm{atm}}$ is the concentration of atmospherically derived helium, including excess air added due to air-water exchange processes, $[^{i}He]_{\mathrm{rad}}$ is the concentration radiogenically derived helium , and $[^{i}He]_{\mathrm{m}}$ is the concentration of magmatic helium for helium isotope i. Helium isotope ratios are commonly reported normalized to the atmospheric ratio:

$$\frac{R}{R_a} = \frac{^{3}He/^{4}He_{\mathrm{samp}}}{^{3}He/^{4}He_{\mathrm{atm}}} \tag{2}$$

where the subscript *samp* is the ratio measured in the sample and subscript *atm* is the atmospheric standard. Radiogenically dominated samples have $R/R_a < 1$, and samples with a magmatic influence have $R/R_a > 1$. Groundwater in volcanic environments commonly shows enrichment above atmospheric equilibrium in both ^{3}He and ^{4}He concentrations. The helium isotope ratio of groundwater depends upon of the amount of crustal (radiogenic) and mantle helium added along the flow path.

3.2. Stream Transport

Groundwater discharging to surface water can change the chemistry and dissolved gas concentration of the surface water. In the case of conservative species such as chloride, the concentration will change according to relatively simple mass balance mixing. In the case of dissolved gases, water will exchange gases with the atmosphere until reequilibration at the local surface water temperature and atmospheric pressure. Gas re-equilibration is limited by the gas exchange velocity which, in the case of flowing streams, means that a groundwater discharge signal can be observed in the stream a finite distance downstream of the discharge point. Radioactive species, such ^{222}Rn, will also undergo radioactive decay in the surface water, decreasing the concentration with time.

In order to simulate the concentration of volcanic tracers in the stream water, we consider a stream transport model that includes groundwater discharge of varying composition, gas exchange with the atmosphere, and first-order decay. In a well-mixed stream, a reasonable assumption for a mountain river, transport is one dimensional. Assuming steady flow over the course of the synoptic period, the steady-state water mass balance equation for the stream is given by

$$\frac{\partial Q}{\partial x} = \frac{Q_{\mathrm{tr}}}{\partial x} + Pw - Ew + q_{\mathrm{gi}} \cdot w - q_{\mathrm{go}} \cdot w - \frac{Q_p}{\partial x}, \tag{3}$$

where Q is the stream discharge (L^3/t), Q_{tr} is the spatially distributed location of tributary discharge (L^3/t), P is the precipitation rate (L/t), E is the evaporation rate (L/t), q_{gi} is the groundwater gain flux (L/t), q_{go} is the groundwater loss flux (L/t), Q_p is the spatially distributed location of stream diversion (L^3/t), and w is the

stream width (L). One-dimensional, steady-state, advective solute transport with gas exchange, radioactive decay, and groundwater exchange can be written

$$\frac{\partial C}{\partial x} = \frac{q_{gi}w}{Q}(C_{gw} - C) - \frac{kw}{Q}\left(C - C_{atm}\right) - \frac{A}{Q}\lambda C + \frac{1}{Q}\frac{Q_{tr}}{\partial x}(C_{tr} - C) + CEw + Pw(C_p - C), \tag{4}$$

where C is the stream concentration (mol/L^3), A is the stream cross-sectional area (L^2), C_{gw} is the local groundwater concentration (mol/L^3), k is the gas exchange velocity (L/t), C_{atm} is the atmospheric equilibrium concentration of the tracer (mol/L^3), λ is the decay coefficient (t^{-1}), C_{tr} is the concentration of the tributary at the confluence (mol/L^3), and all other variables have been defined for equation 3.

4. Numerical Methods

Equations 3 and 4 represent the chemical and water mass balance equations, respectively, and were used to simulate stream discharge, chloride ($[Cl^-]$), conductivity, ^{3}He, ^{4}He, and ^{222}Rn along the reach. The solution to these equations was approximated numerically using an integral finite difference method based on the FiPy python library (Guyer et al., 2009). The 27 km study reach was discretized at 27 m spacing, with the upstream and downstream locations coincident with the furthest upstream and downstream discharge measurement locations. Constant discharge, equal to the measured upstream discharge (0.28 m^3/s), was assigned at the top of the reach, and a zero gradient in discharge was assigned at the bottom of the reach. Constant concentration equal to the measured concentration at the upstream sampling location was assigned at the upstream boundary for each tracer. Zero-gradient concentration boundary conditions were assigned at the downstream location.

4.1. Model Parameterization

Assigned primary parameters in equations 3 and 4 include the atmospheric equilibrium concentration (C_{atm}), the stream channel morphology (w, d), evaporation and precipitation rate (E, P), gas exchange velocity (k), and decay coefficient (λ). Atmospheric equilibrium concentration for ^{222}Rn was assigned to zero. The atmospheric equilibrium concentration for each isotope of helium was calculated using the temperature-dependent solubility (Ballentine and Hall, 1999), the local atmospheric pressure, and the isotope mole fraction in the atmosphere (Porcelli et al., 2002). The average stream temperature (18.6 °C) was used to calculate the equilibrium gas concentration for all stream samples. Atmospheric pressure (P_a) was estimated from an atmospheric lapse rate equation:

$$P_a = \left(\left(1 - \frac{0.0065Ev}{288.15}\right)^{5.2561}\right) * 0.000101325, \tag{5}$$

using the average elevation (Ev) along the reach, which gives an atmospheric pressure of 7.7×10^{-5} GPa. Calculated equilibrium concentrations are $3.5 \cdot 10^{-8}$ ccSTP/g_{H_2O} for ^{4}He and $4.9 \cdot 10^{-14}$ ccSTP/g_{H_2O} for ^{3}He. Stream geometry was linearly interpolated from stream cross sections at discharge measurement locations (Figure 2). A representative evaporation rate was set to 0.29 in./day, the average August evaporation rate for all pan stations in the state of Wyoming (Western Regional Climate Center, 2019). Precipitation P was set to zero as there were no precipitation events before or during the sampling.

The gas exchange velocity is governed by diffusion across the boundary layer between water and the atmosphere and is a function of the gas-dependent diffusion coefficient, the temperature, and the thickness of the boundary layer. Boundary layer thickness is controlled by the interfacial turbulence and water viscosity. The gas exchange velocity for helium and radon was estimated using empirical scaling relationships with stream geometry following Raymond et al. (2012). The Schmidt number (Sc) is the ratio of kinematic viscosity to the aqueous diffusion coefficient and can be used to characterize the gas exchange coefficient. Gas exchange velocities are commonly normalized by gas exchange at a Schmidt number of 600, k_{600}. We estimated the k_{600} for the study reach, using an empirical relationship with stream geometry (velocity, slope, discharge, and average depth) taken from Raymond et al. (2012). We used Equation 7 from Table 2 in Raymond et al. (2012), which has been shown to work well in western U.S. rivers of similar sizes (Hall et al., 2016). Estimated k_{600} values were subsequently scaled to the gas- and temperature-dependent k_{gas} using

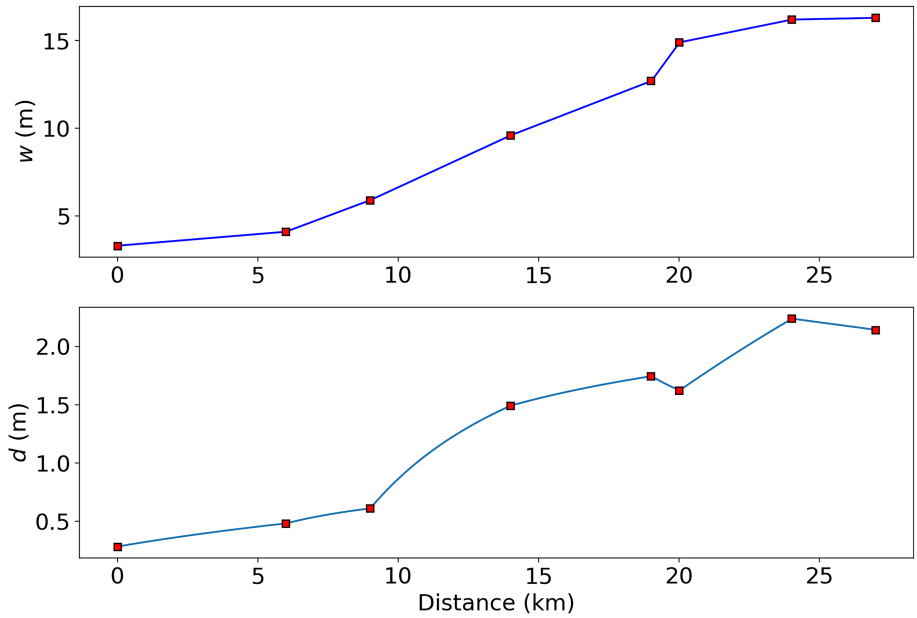

Figure 2. Interpolated stream geometry (blue line) and the measured cross section (red square) width (w) and average depth (d).

Schmidt scaling $\left(k_{\text{gas1}} = \left(\frac{Sc_{\text{gas1}}}{600}\right)^{\frac{1}{2}} k_{600}\right)$ (Jähne and Haußecker, 1998). Schmidt numbers (Sc_{gas}) for helium and radon were calculated using the average stream sampling temperature and equations in Table 1 of Raymond et al. (2012). Calculated gas exchange velocities were 1.5 m/day for ^{222}Rn and 3.8 m/day for ^{3,4}He.

4.2. Modeling Procedure

In the first step, we use our parameterized model to estimate spatially distributed groundwater discharge (q_{gi}), approximated as a step function with eight steps of length 3.4 km. The number of groundwater discharge steps was taken as the number of stream discharge measurement points (8) to keep the inversion problem well posed. The step length was calculated as the total reach length divided by the number of steps. The optimal value of discharge for each step was found using a Levenberg-Marquart optimization routine, which minimized the least-squares residual between modeled and observed stream discharge.

Next, the groundwater composition of helium, chloride, conductivity, and radon (C_{gw_i}) was calculated using the previously calculated best fit groundwater inflow and assuming that groundwater has a spatially constant composition. Groundwater tracer concentrations were estimated by fitting observed synoptic stream concentration for all tracers using a Levenburg-Marquart optimization routine. Parameter estimate uncertainty for all estimated parameters (discharge and concentration) is reported using the linear 95% confidence interval, given the local covariance of the misfit function and the estimated data uncertainty.

5. Synoptic Sampling Methods

We synoptically sampled a 30 km reach of the Gibbon River, beginning ~3 km above the Virginia Cascades, proceeding downstream past the Norris Geyser Basin and ending just above Gibbon Falls (Figure 1). Sampling was conducted during baseflow conditions over a 4 day period in August 2012. Discharge was measured with an acoustic Doppler current profiler (SonTec Flowtracker) at eight locations along the main stem and for five tributaries. Temperature and conductivity were measured and water samples collected for analysis of major ions and dissolved noble gases at 1–2 km intervals. Groundwater springs ranging in temperature from 4 to 90 °C and two local water quality monitoring wells in the Gibbon watershed were sampled over a period of 3 years from 2005 to 2008.

Noble gas samples were collected using equilibrium head space diffusion samplers, equilibrated over a minimum of 24 hr (Gardner and Solomon, 2009). Samples for dissolved ^{222}Rn concentration were collected at

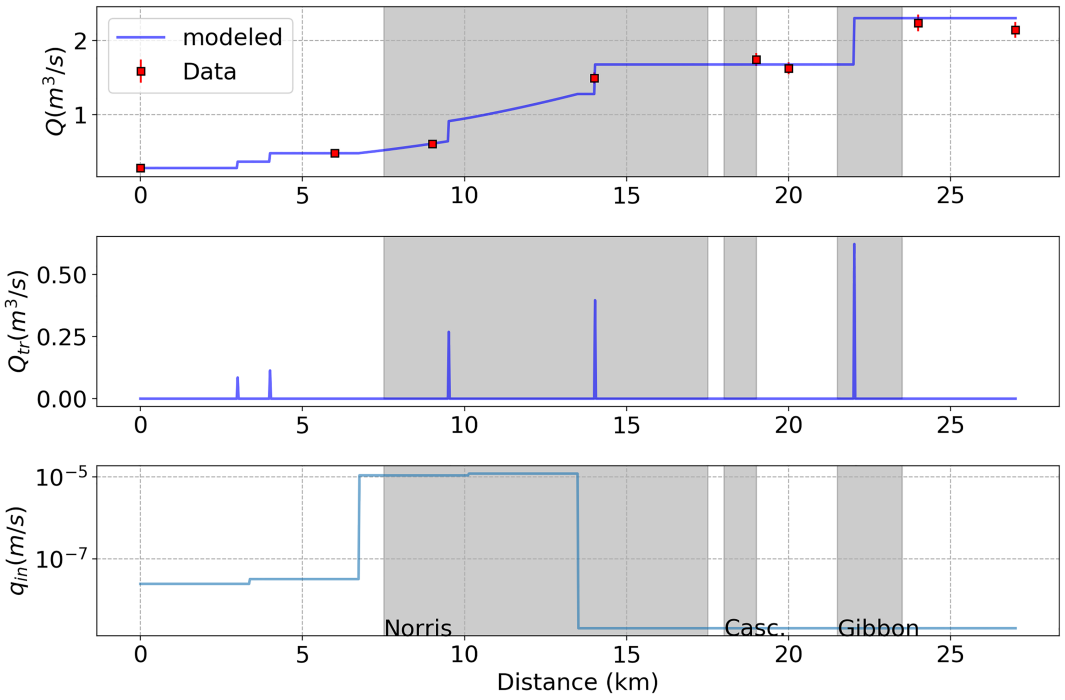

Figure 3. Measured and modeled stream discharge (top), measured tributary discharge (middle), and model-estimated groundwater discharge flux (bottom) for the study reach. Shaded areas represent the location along the reach of the Norris Geyser Basin, a series of small waterfalls and cascades in the canyon below Norris, and the Gibbon Geyser Basin.

~3 km intervals along the reach. Dissolved ion analyses were made using high-pressure liquid chromatography. Dissolved ^{222}Rn concentrations were measured by air sparging and alpha decay spectrometry on site using a RAD7 spectral decay counter. Dissolved noble gas concentration and helium isotopic ratios were measured using mass spectrometry at the University of Utah Dissolved Gas Lab.

6. Results

Measured and modeled stream discharge, measured tributary discharge, and estimated groundwater flux are shown in Figure 3. Measured stream discharge increases from ~0.2 m^3/s at the top of the reach to ~2 m^3/s at the bottom of the reach. Five tributaries come into the Gibbon over the study reach and account for the majority of the stream flow increase. A significant increase in groundwater discharge flux from $\sim 3 \cdot 10^{-8}$ to $\sim 1 \cdot 10^{-5}$ m/s occurs between 7 and 13 km, which corresponds to the area where the Gibbon flows around the Norris Geyser Basin. Groundwater discharge flux drops to $\sim 2 \cdot 10^{-9}$ m/s below Norris. Modeled and measured discharge data show strong agreement over the entire length of the reach.

Measured and modeled chloride and conductivity are shown in Figure 4. Chloride increases roughly monotonically from 1.2 mg/L at the top of the reach to 44 mg/L at the lower end of the reach. The majority of the increase in chloride occurs in the Norris Geyser Basin area. Conductivity changes show similar pattern, increasing from 66 µS/cm at the upstream end to 318 µS/cm at the downstream end. As with chloride, the bulk of the conductivity increase occurs where the Gibbon flows around the Norris Basin. Both increases are coincident with the area of increased groundwater discharge. Modeled chloride and conductivity generally match the observed trends.

Measured and modeled ^{222}Rn is shown in Figure 4. Radon ranges from 0.3 to 2.2 Bq/L over the reach. Radon concentrations are initially low, rise in the area surrounding Norris Geyser Basin, and then generally decrease for the remainder of the study reach. Smaller rises in ^{222}Rn can be seen near the Gibbon Geyser Basin and just before the end of the reach. Dissolved ^{4}He, ^{3}He, and R/R_a are shown in Figure 5. Both ^{4}He and ^{3}He are near-atmospheric equilibrium at the top of the reach, increase in concentration and peak near the Norris Geyser Basin, and generally decrease downstream. Increases in both helium isotopes are seen again near the Gibbon Geyser Basin. Both helium isotopes are significantly enriched above atmospheric

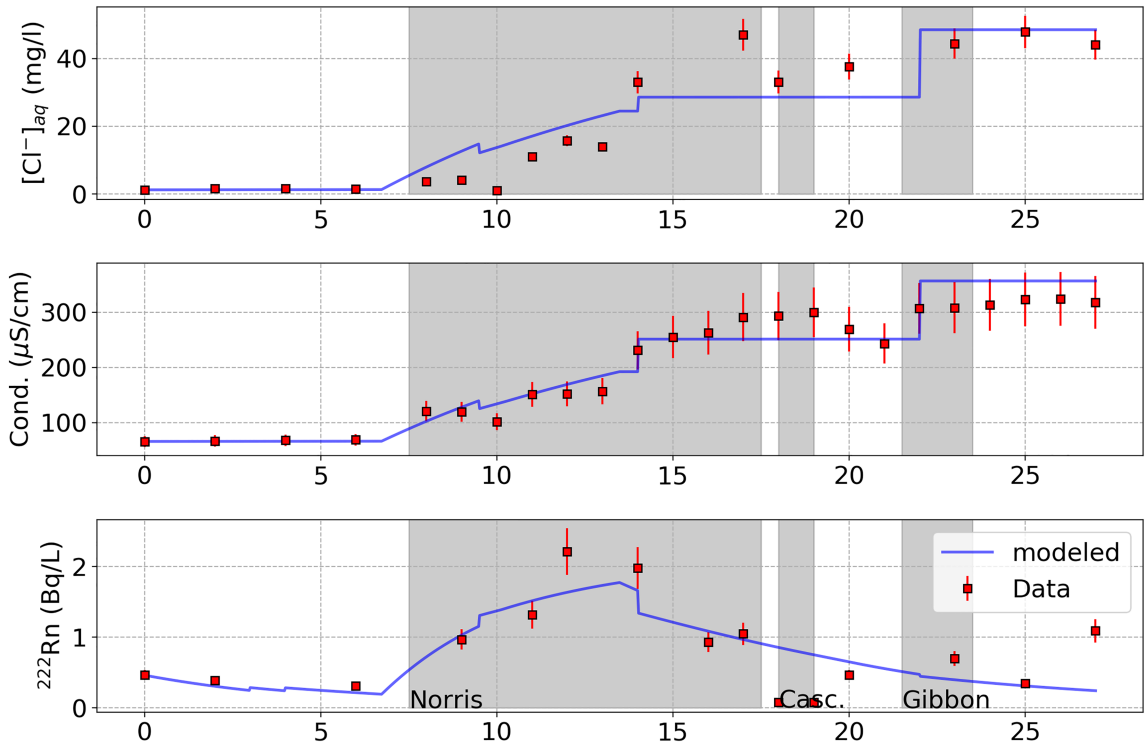

Figure 4. Measured and modeled stream dissolved chloride (top), conductivity (middle), and ^{222}Rn (bottom) for the study reach. Shaded areas represent the location along the reach of the Norris Geyser Basin, a series of small waterfalls and cascades in the canyon below Norris, and the Gibbon Geyser Basin.

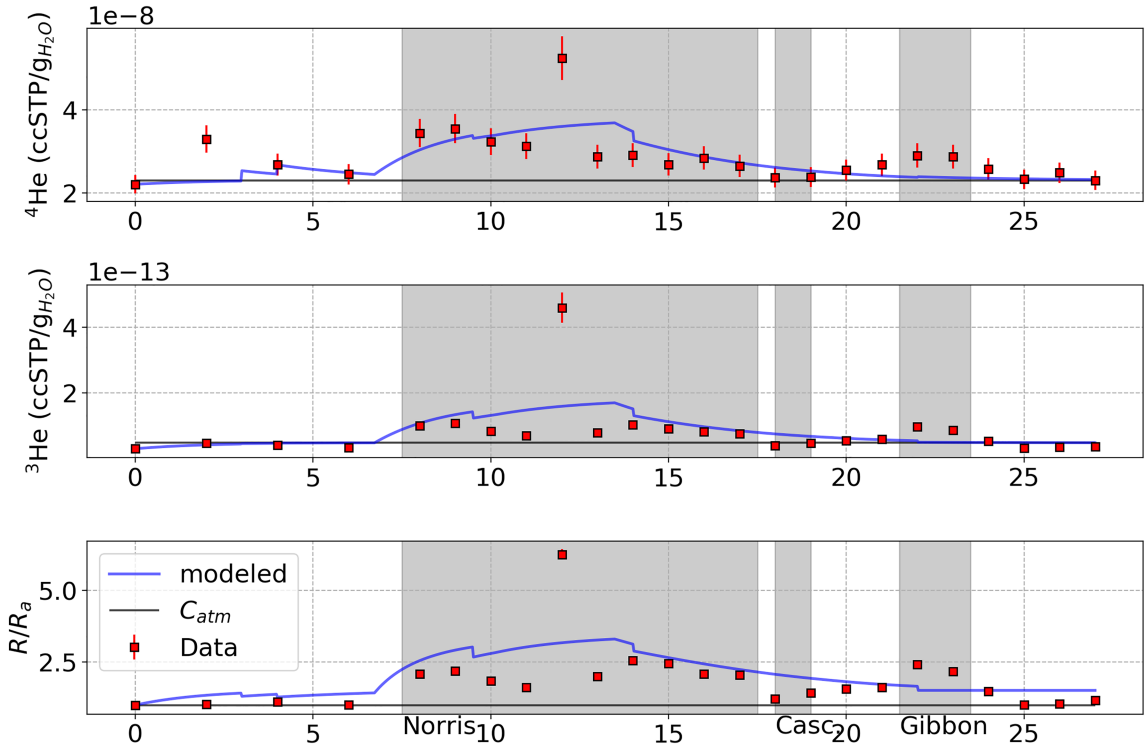

Figure 5. Measured and modeled stream dissolved ^{4}He, (top), ^{3}He (middle), and R/R_a (bottom) for the study reach. Shaded areas represent the location along the reach of the Norris Geyser Basin, a series of small waterfalls and cascades in the canyon below Norris, and the Gibbon Geyser Basin.

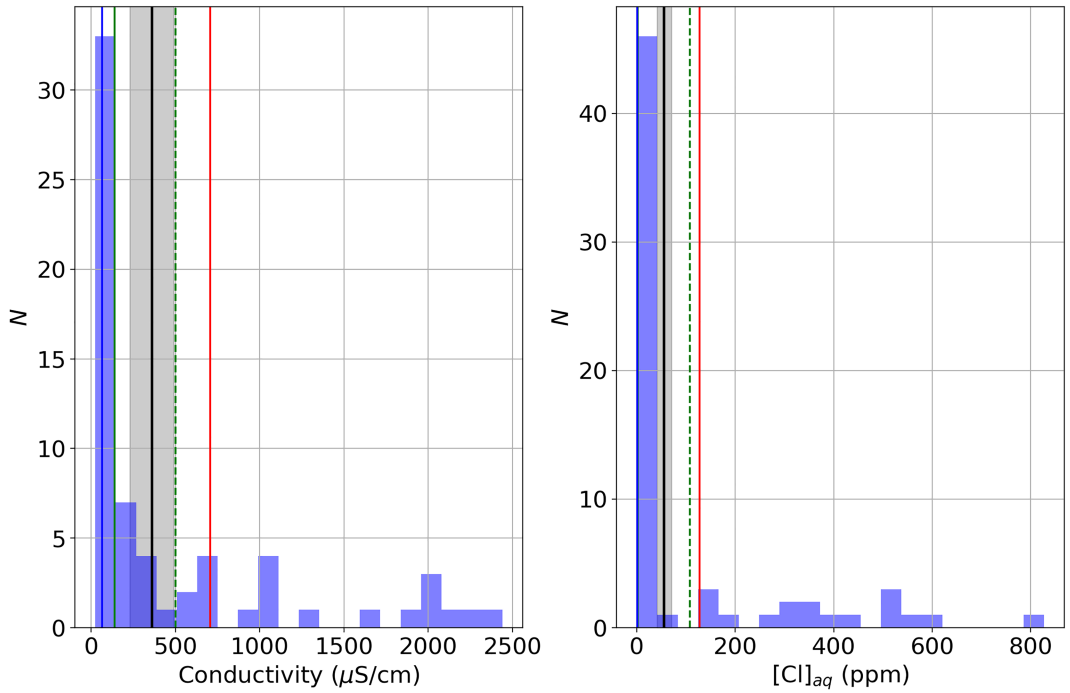

Figure 6. Histogram of groundwater (blue bars) along with the median (solid green line), mean (dashed green line), and 25th (blue line) and 75th (red line) quantiles. Model-estimated groundwater composition is given by the solid black line, and the 95% linear confidence interval of the estimated groundwater composition is shaded in gray. Left panel is for conductivity, and the right panel is for dissolved chloride.

equilibrium—well above analytical error—for the entire region around the Norris Geyser Basin. The R/R_a in the stream is near atmospheric at the top of the reach and rises above 2 for the Norris and Gibbon Geyser Basin sections. Modeled ^{222}Rn, ^{3}He, and ^{4}He capture the gross observed spatial pattern, and all dissolved gases increase in stream water coincident with the groundwater discharge locations and then generally decrease as gas exchange reequilibrates the stream water with the atmosphere.

6.1. Groundwater Comparison

Model-estimated groundwater conductivity was 360 ± 120 μS/cm, chloride was 55 ± 15 mg/L, ^{4}He was $9.2{\cdot}10^{-8}{\pm}3.3{\cdot}10^{-8}$ ccSTP/g_{H_2O}, and ^{3}He was $6.7{\cdot}10^{-13}{\pm}8.7{\cdot}10^{-14}$ ccSTP/g_{H_2O}. The estimated helium isotopic composition of groundwater had an R/R_a of 5.2 ± 2. The uncertainty of the isotope ratio was calculated as $\sigma_{R/R_a} = R/R_a^* \left(\sqrt{\left(\frac{\sigma_{3He}}{[^3He]^*}\right)^2 + \left(\frac{\sigma_{4He}}{[^4He]^*}\right)^2} \right)$, the $\sigma_{x_{He}}$ is the stated uncertainty of the estimated ^{3}He and ^{4}He, and * indicates the model-estimated parameters.

Model-estimated groundwater composition is consistent with groundwater samples from the Norris and Gibbon areas. In Figures 6–8, we plot the distribution and statistics (mean, median, and 25th and 75th percentiles) of groundwater composition from springs in the area, along with model-estimated groundwater concentrations. Our model-estimated groundwater composition agrees well with that measured in springs for all analytes investigated. In all cases, the model-estimated groundwater composition lies within the 25th and 75th quantiles of observed groundwater composition. For both chloride and conductivity, model-estimated groundwater composition lies between the median and mean of sampled groundwater. For both helium isotopes, the model-estimated groundwater concentration is very close to the median groundwater concentration. The estimated R/R_a is higher than both the median and mean groundwater compositions but still falls below the 75th quantile of measured groundwater concentrations in the area.

7. Discussion

The combined signature of stream discharge and volcanic tracers paints a coherent picture of groundwater discharge into the Gibbon River. Near Norris Geyser Basin, an increase in discharge is coincident with a

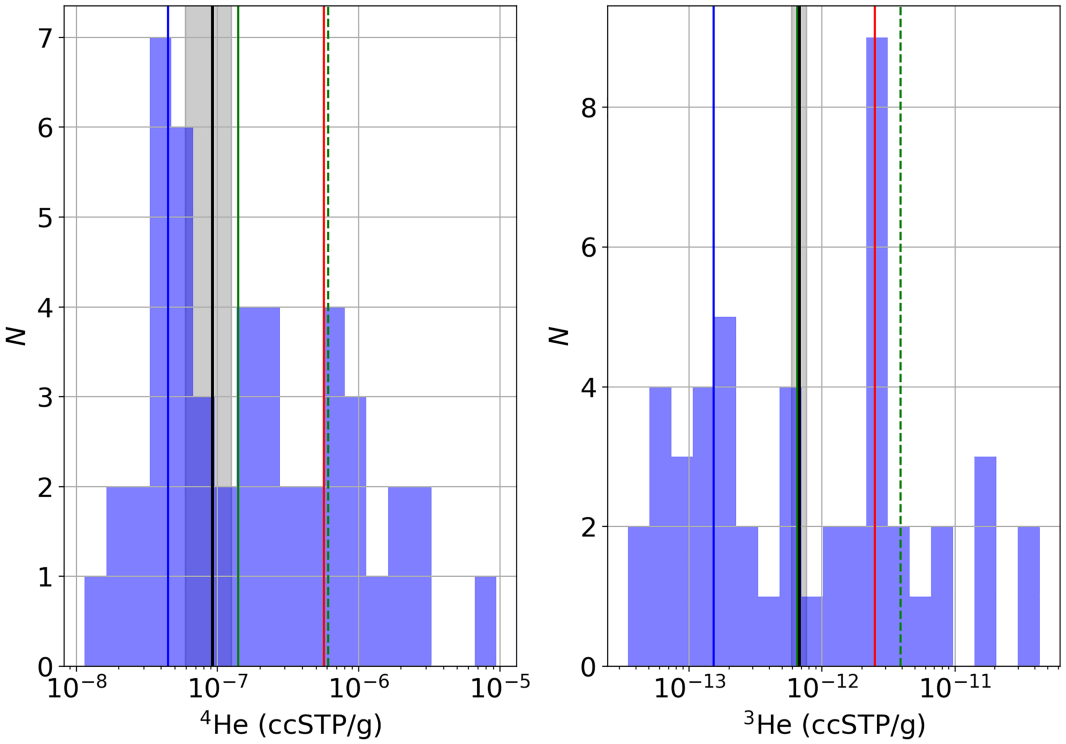

Figure 7. Histogram of sampled groundwater (blue bars) along with the median (solid green line), mean (dashed green line), and 25th (blue line) and 75th (red line) quantiles. Model-estimated groundwater composition is given by the solid black line, and the 95% linear confidence interval of the estimated groundwater composition is shaded in gray. Left panel is for ^{4}He, and the right panel is for ^{3}He. For both panels, the model-estimated groundwater composition line overlays the median groundwater composition.

peak in ^{222}Rn, ^{3}He, ^{4}He, and R/R$_a$ and a rapid rise in chloride (Figures 4 and 5). Model-estimated groundwater discharge shows an influx of groundwater in the area surrounding Norris Geyser Basin. Groundwater discharge to the river appears to be limited downstream of the geyser basin, where dissolved gases reequilibrate with the atmosphere. Our modeling procedure produced groundwater compositions that agree well with those observed in springs and wells in the area. It is clear that the method can be used to broadly characterize the groundwater composition of the region.

Our results indicate that there is excess mantle helium in the Gibbon River (Figures 1 and 5). ^{3}He/^{4}He isotopic ratios in surface water sampled the Gibbon River range from values of 1 (atmospheric equilibrium) up to a high of 6. The majority of samples has a ratio around 2. These values are typical of waters with a large contribution of mantle ^{3}He. Groundwater in the Gibbon River watershed is significantly enriched in helium above atmospheric equilibrium from both crustal (radiogenic) and magmatic sources, with a strong mantle ^{3}He signal (Kennedy et al., 1985). In Figure 9 (left panel), we explore the effect of mixing on the helium isotopic composition and dissolved noble gas composition. We utilize a fractionation factor:

$$F(^4He) = \frac{x_{^4He_s}/x_{^{40}Ar_s}}{x_{^4He_a}/x_{^{40}Ar_a}}, \tag{6}$$

which normalizes the molar ratio of $^4He/^{40}Ar$ measured in the sample (subscript s) by that of the atmosphere (subscript a). The expected isotopic ratio from addition of helium with a R/R_a of 8.5 is plotted on Figure 9 (both panels). This value is representative of mid-ocean ridge basalt (Porcelli et al., 2002) and lies between the average R/R_a of 7 found in the caldera and the R/R_a of 11 found in the Gibbon Geyer Basin (Kennedy et al., 1985). In Figure 9 (right panel), we plot the $^3He/^4He$ ratio versus $^{20}Ne/^4He$ ratio, which allows us to isolate the covariance of ^{3}He (mantle source) and ^{20}Ne (atmospheric source).

From Figure 9, it is clear that the helium concentration and isotopic composition in the Gibbon River falls along the mid-ocean ridge basalt mixing line and contains excess magmatic helium. Helium isotopic values

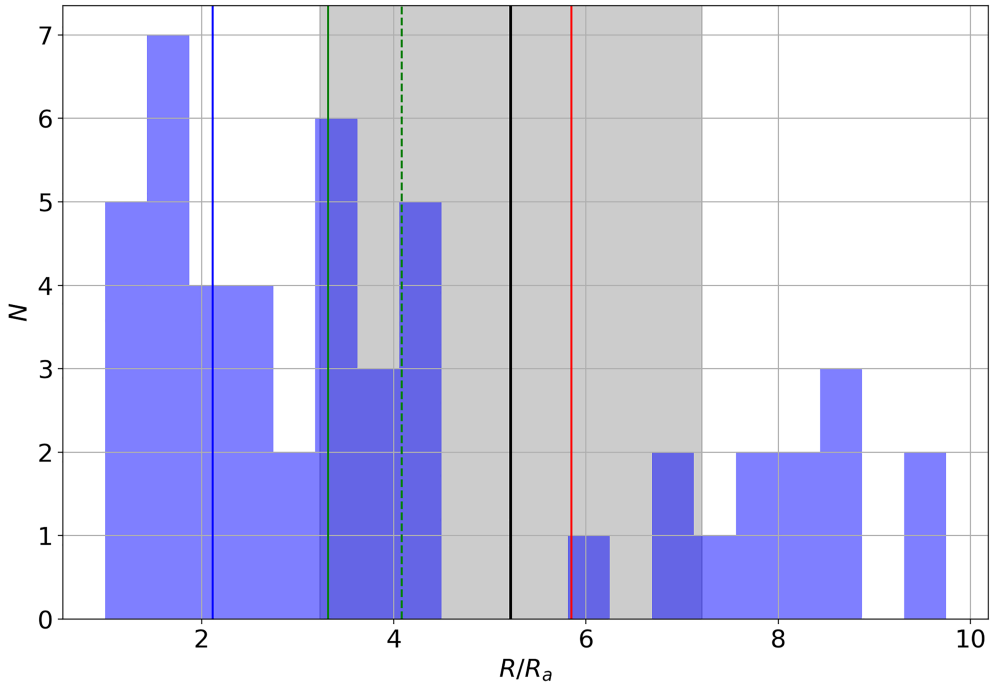

Figure 8. Histogram of sampled groundwater R/R_a (blue bars) along with the median (solid green line), mean (dashed green line), and 25th (blue line) and 75th (red line) quantiles. Model-estimated groundwater R/R_a is given by the solid black line, and the 95% linear confidence interval of the estimated groundwater composition is shaded in gray.

and mixing trends are broadly consistent with groundwater compositions observed in Norris area; however, stream samples show less crustal influence than many springs. These results indicate that a strong volcanic volatile signal can be observed in the stream water. This volcanic signal persists several kilometers downstream of the main input location.

7.1. Caveats and Limitations

Downstream of the Norris Geyser Basin, the Gibbon River enters a narrow canyon and steeply descends over a series of cascades before reaching the Gibbon Geyser Basin. This cascade section of the river is marked by very shallow depth of water (<0.25 m), enhanced velocity, turbulence, and bubble entrainment (whitewater). The two samples from this canyon reach have low to no ^{222}Rn and atmospheric levels of helium, indicative of rapid air-water exchange and reequilibration in this section of the river. The assumption of a single gas exchange coefficient likely leads to significant error in modeling in these reaches.

Groundwater discharge to streams integrates many flow paths and sources. The distribution of groundwater discharge is likely to vary significantly along a stream reach due to changes in the subsurface structure and the underlying hydrogeologic system (e.g., Gardner et al., 2011a). Thus, our assumption of a single groundwater composition along the reach is likely not accurate. The composition of groundwater for each discharge step could potentially be treated as individual parameters, allowing one to estimate the spatially distributed groundwater composition, increasing the spatial resolution of the method. This increase in spatial resolution would come at the cost of parameter parsimony, increased numerical burden during the model inversion, and potential for over fitting. The objective of this initial study is to demonstrate the potential for this method to characterize the average groundwater composition. Further refinement in methods and data collection could be used to improve the spatial resolution of estimated groundwater composition.

The quality of the fit for helium species, in particular, is not as good as that for the dissolved ionic species. Several reasons could explain the poor fit for helium isotopes. First, our model only considers helium added to stream water via groundwater discharge. Helium added as a result of in-stream gas phase fumerols, which change helium composition of the stream without affecting discharge and other dissolved species, could be a source of error. Second, as discussed above, a single groundwater composition was assumed for helium concentration and isotopic composition. Given the 3 order of magnitude variation in observed concentration

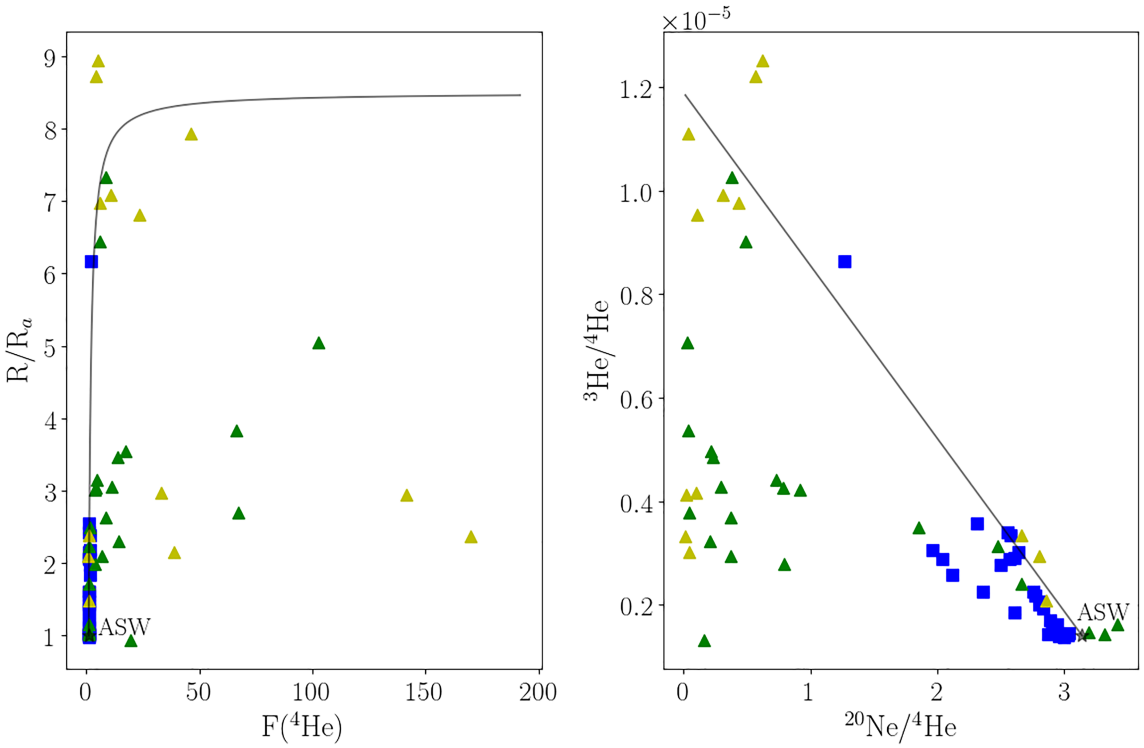

Figure 9. (left) Helium R/R_a versus helium fractionation factor $F(^4He)$ (equation (6)) for all stream water samples (blue squares), springs less than 20 °C (green triangles), and springs greater than 20 °C (yellow triangles). (right) $^4He/^3He$ versus $^{20}Ne/^4He$ for all stream water samples (blue squares), springs less than 20 °C (green triangles), and springs greater than 20 °C (yellow triangles). Mixing lines starting at atmospheric composition (black star = ASW) and adding helium with an R/R_a of 8.5 are plotted in black.

for each helium isotope (Figures 7 and 8), it is likely that a large source of misfit is the assumption of single groundwater end-member composition.

The stream survey and sampling occurred over the course of a week of field work, whereas it took roughly three summers of field work to locate and sample all the springs in the area. The stream survey method is a highly efficient method to characterize the groundwater system across a large spatial area. In addition, the Gibbon River just downstream of the Norris Geyser Basin retains the helium composition from a large (~7 km) stream reach and thus integrates many discharge features. Rather than sampling individual springs and thermal features, which relies on point features being connected to a subsurface disturbance, stream sampling could potentially be used to monitor a much large geographic area, with a greater chance of detecting changes.

Helium has distinct isotopic signatures for magmatic and crustal processes, has a high molecular diffusivity, does not react with or sorb to mineral surfaces, and is among the more mobile elements in the subsurface with (Porcelli et al., 2002). The concentration helium in stream water provides a convenient method to monitor a spatially integrated signal of groundwater composition over a large spatial extent. Chloride concentration in surface water is used to monitor volcanic systems and hydrothermal systems (Ingebritsen et al., 2001; Norton and Friedman, 1985). Chloride is a conservative tracer, but has a long residence time in surface water catchments and can be contributed by a variety of surficial sources. In contrast to Cl^-, magmatic helium has a very short residence time in surface water due to atmospheric exchange, eliminating the ambiguity of the source. Monitoring magmatic helium in stream water could potentially be a tool for monitoring changes in the volcanic and hydrothermal systems.

8. Conclusion

We provide the first evidence that elevated magmatic helium from groundwater discharge can be measured in stream water, with a demonstration in the Gibbon River near Norris Geyser Basin in Yellowstone National Park. Large peaks in ^3He concentrations can be seen in stream water and persist over 5 km downstream.

These peaks in ^{3}He are broadly consistent with peaks in ^{222}Rn and increases in stream chloride concentrations. We show that the data can be used to estimate both the volume and the composition of groundwater discharge, by inverting a model of stream flow and transport against the combined observations of stream discharge, Cl^{-}, ^{222}Rn, and helium isotopic composition. The estimated groundwater composition has a strong magmatic signal and compares well with springs near the Gibbon River. The results clearly demonstrate that: (1) the stream water helium isotopes differ significantly from air saturated water, consistent with the addition of helium from a mantle magmatic source and (2) our modeling procedure allows us to characterize the groundwater composition from a synoptic stream survey alone. Our initial study indicates that magmatic ^{3}He measured in stream water could potentially be a new tool for monitoring changes in the volcanic system and that further research into long-term monitoring of stream water helium in volcanic systems is warranted.

Appendix A: Groundwater Spring Data Retrieval

Spring chemistry data from this project are stored on the USGS National Water Information System (NWIS). These electronic data files can be easily accessed from the NWIS web interface. This section provides instructions on how to retrieve and download the data from the NWIS web interface using the USGS site identification numbers for each site. A list of site identification numbers for all sites created for this study is given in Table A1. Several sites were sampled multiple times. These sites will have multiple records with unique dates. Not all parameters were analyzed at each site for a given sampling time.

Use a file containing all the sites created to query all the data at once. To do this, create a tab delimited text file that looks just like the body of Table A1 that contains all the site numbers for which data are desired. This file should contain no header line and have all site numbers for which data are wanted. Once this file has been created, save it in a known location. Downloading the site information and data is now quick and easy.

These instructions are valid for a batch download of all data from the NWIS web system as of 25 May 2009, using a tab delimited file of site numbers. The web interface changes periodically, and downloading may change in the future; however, the station numbers will not change, and the data will be available in perpetuity.

Point your browser to the USGS NWIS web site at http://waterdata.usgs.gov/nwis and select the "Water Quality" link. From here, select the "Field/Lab Samples" link. Select a site selection criteria of "File of Site Numbers" under "Site Identifier" column and click on the "Submit" button. Click on the "Choose File" button underneath the "File of Site Numbers" header and browse to the location of text file made above. From here, there are many options—you can view site information, sampling times, and so forth for any

Table A1
List of USGS Site ID Numbers for Sampling Sites Created as a Part of This Study

Agency	Station number
USGS	443002111151801
USGS	443334110241001
USGS	443337110240501
USGS	443708110505501
USGS	444007110443301
USGS	444044110444701
USGS	444136110430201
USGS	444138110435801
USGS	444151110430101
USGS	444236110442801
USGS	444240110392001
USGS	444242110394701
USGS	444243110383801
USGS	444243110394701

Table 1
Continued

Agency	Station number
USGS	444243110400901
USGS	444246110384801
USGS	444310110415401
USGS	444311110430001
USGS	444320110420801
USGS	444324110375501
USGS	444340110420201
USGS	444347110413601
USGS	444351110400801
USGS	444353110422301
USGS	444409110430101
USGS	444410110422301
USGS	444412110420601
USGS	444415110351801
USGS	444420110430001
USGS	444423110411001
USGS	444423110425801
USGS	444424110411801
USGS	444425110403001
USGS	444438110405901
USGS	444443110404501
USGS	444444110433301
USGS	444500110433801
USGS	444528110435901
USGS	444700110415101
USGS	444709110420001
USGS	444711110442701
USGS	445105110440701
USGS	445308111031401
USGS	445726110484101
USGS	445820110462201

Note. Many sites were sampled more than once and will have several data records for a single site each with different sampling dates.

site number given. To download an electronic file for all sites given in Table A1, select the "Tab separated

data" radio button. The default parameters are sufficient as they are. The file is not large, so a compressed file is not needed. Click the "Submit" button, file named *"qwdata"* should either be downloaded directly or you should be prompted on where to save this file. This file is a tab delimited text file with all parameters, parameter codes, parameter code descriptions and data. Have fun!

References

Aeschbach-Hertig, W., El-Gamal, H., Wieser, M., & Palcsu, L. (2008). Modeling excess air and degassing in groundwater by equilibrium partitioning with a gas phase. *Water Resources Research*, *44*, 1–12. https://doi.org/10.1029/2007WR006454

Aeschbach-Hertig, W., Peeters, F., Beyerle, U., & Kipfer, R. (2000). Paleotemperature reconstruction from noble gases in ground water taking into account equilibration with entrapped air. *Nature*, *405*, 1040–1044.

Aizawa, K., Sumino, H., Uyeshima, M., Yamaya, Y., Hase, H., Takahashi, H. A., et al. (2016). Gas pathways and remotely triggered earthquakes beneath Mount Fuji, Japan. *Geology*, *44*(2), 127–130. https://doi.org/10.1130/G37313.1

Allard, P., Jean-Baptiste, P., D'Alessandro, W., Parello, F., Parisi, B., & Flehoc, C. (1997). Mantle-derived helium and carbon in groundwaters and gases of Mount Etna, Italy. *Earth and Planetary Science Letters*, *148*(3-4), 501–516. https://doi.org/10.1016/S0012-821X(97)00052-6

Allen, E. T., & Day, A. L. (1935). Hot springs of the Yellowstone National Park. *Carnegie Institution of Washington Publication*, *466*, 525.

Ballentine, C. J., Burgess, R., & Marty, B. (2002). Tracing fluid origin and interaction in the crust. In D. Porcelli, C. J. Ballentine, & R. Wieler (Eds.), *Noble gases in geochemistry and cosmochemistry, Reviews in Minerology and Geochmistry*, (chap. 13, Vol. 47, pp. 539–614). Washington, DC: Mineralogical Society of America.

Ballentine, C. J., & Hall, C. M. (1999). Determining paleotemperature and other variables by using error-weighted, nonlinear inversion of noble gas concentrations in water. *Geochimica et Cosmochimica Acta*, *63*(16), 2315–2336.

Bauer, S., Gardner, W., & Heath, J. (2016). Helium release during shale deformation: Experimental validation. *Geochemistry, Geophysics, Geosystems*, *17*, 2612–2622. https://doi.org/10.1002/2016GC006352

Bauer, S., Gardner, W., & Lee, H. (2016). Release of radiogenic noble gases as a new signal of rock deformation. *Geophysical Research Letters*, *43*, 10,688–10,694. https://doi.org/10.1002/2016GL070876

Bauer, S. J., Gardner, W. P., & Lee, H. (2019). Noble gas release from bedded rock salt during deformation. *Geofluids*, *2019*, 12. https://doi.org/10.1155/2019/2871840

Beisner, K. R., Gardner, W. P., & Hunt, A. G. (2018). Geochemical characterization and modeling of regional groundwater contributing to the Verde River Arizona between Mormon Pocket and the USGS Clarkdale gage. *Journal of Hydrology*, *564*, 99–114. https://doi.org/10.1016/J.JHYDROL.2018.06.078

Brauer, K., Kampf, H., Strauch, G., & Weise, S. M. (2003). Isotopic evidence (He-3/He-4, C-13(CO_2)) of fluid-triggered intraplate seismicity. *Journal of Geophysical Research*, *108*(B2), 2070. https://doi.org/10.1029/2002JB002077

Cook, P. G., Favreau, G., Dighton, J. C., & Tickell, S. (2003). Determining natural groundwater influx to a tropical river using radon, chloroflourocarbons and ionic environmental tracers. *Journal of Hydrology*, *277*(1-2), 74–88. https://doi.org/10.1016/S0022-1694(03)00087-8

Cook, P. G., Lamontagne, S., Berhane, D., & Clark, J. F. (2006). Quantifying groundwater discharge to Cockburn River, southeastern Australia, using dissolved gas tracers ^{222}Rn and SF_6. *Water Resources Research*, *42*, 1–12. https://doi.org/10.1029/2006WR004921

Crankshaw, I., Archfield, S., Newman, A., Bergfeld, D., Clor, L., Spicer, K., et al. (2018). Multi-year high-frequency hydrothermal monitoring of selected high-threat Cascade Range volcanoes. *Journal of Volcanology and Geothermal Research*, *356*, 24–35. https://doi.org/10.1016/J.JVOLGEORES.2018.02.014

Despain, D. G. (1987). The two climates of Yellowstone National Park. *Proceedings of the Montana Academy of Science*, *47*, 11–19.

Fournier, R. O. (1989). Geochemistry and dynamics of the Yellowstone National Park hydrothermal system. *Annual Review of Earth and Planetary Sciences*, *17*(1), 13–53. https://doi.org/10.1146/annurev.ea.17.050189.000305

Friedman, I., & Norton, D. R. (1990). Anomalous chloride flux discharges from Yellowstone National Park. *Journal of Volcanology and Geothermal Research*, *42*(3), 225–234. https://doi.org/10.1016/0377-0273(90)90001-V

Gardner, P., & Solomon, D. K. (2009). An advanced passive diffusion sampler for the determination of dissolved gas concentrations. *Water Resoures Research*, *45*, W06423. https://doi.org/10.1029/2008WR007399

Gardner, W. P., Susong, D., Solomon, D., & Heasler, H. (2011a). A multitracer approach for characterizing interactions between shallow groundwater and the hydrothermal system in the Norris Geyser Basin area, Yellowstone National Park. *Geochemistry, Geophysics, Geosystems*, *12*, Q08005. https://doi.org/10.1029/2010GC003353

Gardner, W. P., Bauer, S. J., Kuhlman, K. L., & Heath, J. E. (2017). Modeling dynamic helium release as a tracer of rock deformation. *Journal of Geophysical Research: Solid Earth*, *122*, 8828–8838. https://doi.org/10.1002/2017JB014376

Gardner, W. P., Susong, D. D., Solomon, D. K., & Heasler, H. P. (2010a). Snowmelt hydrograph interpretation: Revealing watershed scale hydrologic characteristics of the Yellowstone Volcanic Plateau. *Journal of Hydrology*, *383*(3-4), 209–222. https://doi.org/10.1016/j.jhydrol.2009.12.037

Gardner, W. P., Susong, D. D., Solomon, D. K., & Heasler, H. P. (2010b). Using noble gases measured in spring discharge to trace hydrothermal processes in the Norris Geyser Basin, Yellowstone National Park, U.S.A. *Journal of Volcanology and Geothermal Research*, *198*(3-4), 394–404. https://doi.org/10.1016/j.jvolgeores.2010.09.020

Gardner, W. P., Susong, D. D., Solomon, D. K., & Heasler, H. P. (2013). Using environmental tracers and numerical simulation to investigate regional hydrothermal basins—Norris Geyser Basin area, Yellowstone National Park, USA. *Journal of Geophysical Research: Solid Earth*, *118*, 2777–2787. https://doi.org/10.1002/jgrb.50210

Guyer, J. E., Wheeler, D., & Warren, J. A. (2009). FiPy: Partial differential equations with Python. *Computing in Science & Engineering*, *11*(3), 6–15. https://doi.org/10.1109/MCSE.2009.52

Hall, R. O., Tank, J. L., Baker, M. A., Rosi-Marshall, E. J., & Hotchkiss, E. R. (2016). Metabolism, gas exchange, and carbon spiraling in rivers. *Ecosystems*, *19*(1), 73–86. https://doi.org/10.1007/s10021-015-9918-1

Hurwitz, S., Christiansen, L. B., & Hsieh, P. A. (2007). Hydrothermal fluid flow and deformation in large calderas: Inferences from numerical simulations. *Journal of Geophysical Research*, *112*, B02206. https://doi.org/10.1029/2006JB004689

Hurwitz, S., Ingebritsen, S. E., & Sorey, M. L. (2002). Episodic thermal perturbations associated with groundwater flow: An example from Kilauea Volcano, Hawaii. *Journal of Geophysical Research*, *107*(B11), 2297. https://doi.org/10.1029/2001JB001654

Acknowledgments

The authors would like to thank Dan Mahoney for his help and wit in the field and Hank Heasler for his devotion to research in the Park. All groundwater sample data are permanently stored on the USGS NWIS database. Detailed instructions for download are given in Appendix A. Stream sampling data and meta data as well as the input decks and a copy of the code used to produce the results can be viewed and downloaded online (https://scholarworks.umt.edu/geosci_data/3). The code is provided as is and will require the user to install the required python libraries.

Hurwitz, S., Kipp, K. L., Ingebritsen, S. E., & Reid, M. E. (2003). Groundwater flow, heat transport and water table position within volcanic edifices: Implications for volcanic processes in the Cascade Range. *Journal of Geophysical Research*, *108*(B12), 2557. https://doi.org/10.1029/2003JB002565

Hutnak, M., Hurwitz, S., Ingebritsen, S. E., & Hsieh, P. A. (2009). Numerical models of caldera deformation: Effects of multiphase and multicomponent hydrothermal fluid flow. *Journal of Geophysical Research*, *114*, B04411. https://doi.org/10.1029/2008JB006151

Ingebritsen, S., Galloway, D., Colvard, E., Sorey, M., & Mariner, R. (2001). Time-variation of hydrothermal discharge at selected sites in the western United States: Implications for monitoring. *Journal of Volcanology and Geothermal Research*, *111*(1-4), 1–23. https://doi.org/10.1016/S0377-0273(01)00207-4

Ingebritsen, S. E., & Scholl, M. A. (1993). The hydrogeology of the Kilauea Volcano. *Geothermics*, *22*(4), 255–270.

Jähne, B., & Haußecker, H. (1998). Air-water gas exchange. *Annual Review of Fluid Mechanics*, *30*(1), 443–468. https://doi.org/10.1146/annurev.fluid.30.1.443

Kennedy, B. M., Lynch, M. A., Reynolds, J. H., & Smith, S. P. (1985). Intensive sampling of noble gases in fluids at Yellowstone: I. Early overview of the data; regional patterns. *Geochimica et Cosmochimica Acta*, *49*, 1251–1261.

Kennedy, B. M., & van Soest, M. C. (2007). Flow of mantle fluids through the ductile lower crust: Helium isotope trends. *Science*, *318*(5855), 1433–1436. https://doi.org/10.1126/science.1147537

Lowenstern, J. B., Evans, W. C., Bergfeld, D., & Hunt, A. G. (2014). Prodigious degassing of a billion years of accumulated radiogenic helium at Yellowstone. *Nature*, *506*(7488), 355–358.

Manga, M. (1996). Hydrology of spring dominated streams in the Oregon Cascades. *Water Resources Research*, *32*(8), 2432–2439.

Manga, M. (2001). Using springs to study groundwater flow and active geologic processes. *Annual Reviews of Earth Planet Science*, *29*, 201–228.

McCleskey, R. B., Lowenstern, J. B., Schaper, J., Nordstrom, D. K., Heasler, H. P., & Mahony, D. (2016). Geothermal solute flux monitoring and the source and fate of solutes in the Snake River Yellowstone National Park, WY. *Applied Geochemistry*, *73*, 142–156. https://doi.org/10.1016/J.APGEOCHEM.2016.08.006

Morikawa, N., Kazahaya, K., Fourre, E., Takahashi, H. A., Jean-Baptiste, P., Ohwada, M., et al. (2008). Magmatic He distribution around Unzen volcano inferred from intensive investigation of helium isotopes in groundwater. *Journal of Volcanology and Geothermal Research*, *175*, 218–230. https://doi.org/10.1016/j.jvolgeores.2008.03.038

Norton, D. R., & Friedman, I. (1985). Chloride flux out of Yellowstone National Park. *Journal of Volcanology and Geothermal Research*, *26*(3-4), 231–250. https://doi.org/10.1016/0377-0273(85)90058-7

Ohwada, M., Kazahaya, K., Itoh, J., Morikawa, N., Takahashi, M., Takahashi, H. A., et al. (2012). Passive degassing of magmatic volatiles from Iwate volcano, NE Japan, based on three-dimensional measurement of helium isotopes in groundwater. *Journal of Geophysical Research*, *117*, B02204.

Padrón, E., et al. (2013). Diffusive helium emissions as a precursory sign of volcanic unrest. *Geology*, *41*(5), 539–542. https://doi.org/10.1130/G34027.1

Porcelli, D., Ballentine, C. J., & Wieler, R. (Eds) (2002). Noble gases in geochemistry and cosmochemistry, Reviews in Mineralogy and Geochemistry, (Vol. 47). Washington D.C: Mineralogical Society of America.

Raymond, P. A., Zappa, C. J., Butman, D., Bott, T. L., Potter, J., Mulholland, P., et al. (2012). Scaling the gas transfer velocity and hydraulic geometry in streams and small rivers. *Limnology and Oceanography: Fluids and Environments*, *2*(1), 41–53. https://doi.org/10.1215/21573689-1597669

Saar, M. O., Castro, M. C., & Hall, C. M. (2005). Quantifying magmatic, crustal, and atmospheric helium contributions to volcanic aquifers using all stable noble gases: Implications for magmatism and groundwater flow. *Geochemistry, Geophysics, Geosystems*, *6*, Q03008. https://doi.org/10.1029/2004GC000828

Sano, Y., Kagoshima, T., Takahata, N., Nishio, Y., Roulleau, E., Pinti, D. L., & Fischer, T. P. (2015). Ten-year helium anomaly prior to the 2014 Mt Ontake eruption. *Scientific Reports*, *5*, 13,069.

Smerdon, B. D., Gardner, W. P., Harrington, G. A., & Tickell, S. J. (2012). Identifying the contribution of regional groundwater to the baseflow of a tropical river (Daly River, Australia). *Journal of Hydrology*, *464-465*, 107–115.

Torgersen, T. (1980). Controls on pore-fluid concentration of ^{4}He and ^{222}Rn and the calculation of $^{4}He/^{222}Rn$ ages. *Journal of Geochemical Exploration*, *13*(1), 57–75. https://doi.org/10.1016/0375-6742(80)90021-7

Wanninkhof, R., Mulholland, P. J., & Elwood, J. W. (1990). Gas exchange rates for a first-order stream determined with deliberate and natural tracers. *Water Resoures Research*, *26*(7), 1621–1630.

Western Regional Climate Center (2019), Evaporation stations.

White, D. E., Fournier, R. O., Muffler, L. J. P., & Truesdell, A. H. (1975). Physical results of research drilling in thermal waters of {Y}ellowstone {N}ational {P}ark, {W}yoming. *U.S. Geological Survey Professional Paper*, (892), 70.

White, D. E., Hutchinson, R. A., & Keith, T. E. C. (1988). The geology and remarkable thermal activity of Norris Geyser Basin, Yellowstone National Park, Wyoming. *U.S. Geological Survey Professional Paper*, *1456*.